Analysis of Coupler for Wireless Power Transmission

Kaidong Sun
School of Mechatronic Engineering
Xi`an Technological University
Xi'an, China
E-mail: 1356058684@qq.com

Hao Lai
Academy of Aerospace Solid Propulsion Technology
AASPT
Xi'an, China
E-mail: 15909200228@163.com

Yueshen Lai
School of Mechatronic Engineering
Xi`an Technological University
Xi'an, China
E-mail: lailiquan@xatu.edu.cn

Changke Liu
School of Mechatronic Engineering
Xi`an Technological University
Xi'an, China
E-mail: 1054462088@qq.com

***Abstract*—In the research on wireless power transmission, coupler with the advantages of high transmission power, high charging gap and anti-offset are the hot topics in the current research. Based on Biot-Savart Law, this paper studies the spatial magnetic field distribution characteristics of circular coils and DD coils, and establishes a magnetic field model of coils to achieve a visual analysis of magnetic fields.**

Keywords-WPT; Biot-Savart Law; DD Coils

I. INTRODUCTION

WPT(Wireless Power Transmission) has the advantages of safe operation, flexibility[1], convenience and low maintenance cost, and has important application value in the field of consumer electronics and some coal mines[2], in addition, WPT solves the interface restrictions, charging safety and other problems faced by traditional conductive charging. and become one of the future trends in the development of power transmission technology[3]

As a key component of WPT, the shape and size parameters of coils have a great influence on the performance of the system. Traditional coil design methods rely on engineers' design experience and often require experimental platform and continuous experimentation. In this paper, the magnetic field distribution model of coils is derived from Biot-Savart Law, and the magnetic field distribution characteristics of different coils are analyzed according to the model.

The law of Biot-Savart is the basic theorem for the magnetic field that is excited by current elements at any point in space. It expounds the mathematical relationship between the linear current and the magnetic field strength it produces, and its mathematical expression is as follows[4]

$$d\vec{B}=\frac{\mu_0 I}{4\pi}\frac{dlR^0}{R^3} \tag{1}$$

In the formula:

I —Current value of flowing through the coil;

dl —The unit length of the linear current;

R —Distance from the line current of the unit length to the target point;

R^0 —The unit vector of the unit length of the linear current pointing to the target point;

dB —Magnetic induction intensity generated at the target point by a linear current of a unit length。

Based on the law of Biot-Savart, the Magnetic induction intensity of each point in the rectangular coordinate system can be obtained by mathematical derivation according to the geometric model of the coil. In this paper, the magnetic field distribution of the circular coil is analyzed, and then the magnetic field distribution of the DD coil in space is given.

II. MAGNETIC INDUCTION INTENSITY DISTRIBUTION OF CIRCULAR COILS

When solving the magnetic field of the space in which the coil is located, the meshing of the space in which the coil is located is first meshed in the coordinate system, and the magnetic field distribution of the coil in each mesh is analyzed. Theoretically, when the grid edge long value is close to 0, the result of the calculation will be infinitely close to the actual value. However, to avoid excessive calculations that make it difficult to get results, the grid cannot be taken too small. the center of the coil geometry coincides with the coordinate system origin and divides the circumpolarity of the circular coil into N equal parts, each with a length of $\Delta l_n=(2\pi/N)\cdot R$ and the length of the entire coil $2\pi R$. Set R_n to target point P to each cell length Δl_n distance, R_n^0 is the unit length of each unit point to target point P unit vector. The relationships between the variables are shown in Figure 1.

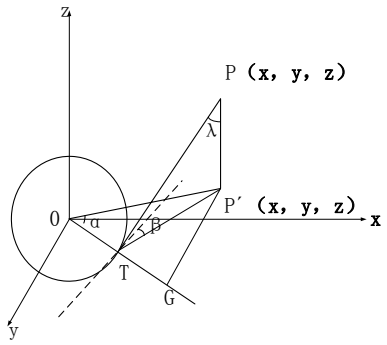

Figure 1. Magnetic induction intensity analysis of circular coils

The coordinates of the observation point are $P(x,y,z)$ and the distance between observation point P and Δl_n is R_n. For ease of calculation, take the end point of each Δl_n to calculate the distance, and set the unit vector for each Δl_n to P to R_n^0. For illustration purposes, place observation point P on a parallel plane with a distance of H from the coil, and project P point onto the coil plane, with a projection of P at P'. Since PP' and the coil plane are vertical, these 3 points of P, P', T constitute a right triangle, and PT is an oblique.

The distance from point P to Δl_n is R_n:

$$R_n = (PP'^2 + P'T^2)^{\frac{1}{2}} \tag{2}$$

Since,

$$PT = R_n = (z^2 + x^2 + y^2 + R^2 - 2R\sqrt{x^2+y^2}\cdot\cos(n\cdot\frac{2\pi}{N}))^{\frac{1}{2}} \tag{3}$$

And,

$$R_n^0 = \sin\lambda_n \sin\beta_n = \frac{TP'}{PT}\cdot\frac{TG}{TP'} = \frac{TG}{PT} \tag{4}$$

Thus,

$$R_{n0}^0 = \frac{\sqrt{x^2+y^2}\cdot\cos(n.\frac{2\pi}{N}) - R}{(z^2 + x^2 + y^2 + R^2 - 2R\sqrt{x^2+y^2}\cdot\cos(n\cdot\frac{2\pi}{N}))^{\frac{1}{2}}} \tag{5}$$

According to Formula,

$$\Delta B_P = \frac{\mu_0 I}{4\pi}\frac{dlR^0}{R^3} \tag{6}$$

$$\Delta H_P = \frac{IR}{2N}\frac{\sqrt{x^2+y^2}\bullet\cos(n\bullet\frac{2\pi}{N}) - R}{(z^2 + R^2 + x^2 + y^2 - 2R\sqrt{x^2+y^2}\bullet\cos(n\bullet\frac{2\pi}{N}))^{\frac{3}{2}}} \tag{7}$$

The magnetic induction intensity of point P is B_P,

$$B_P = \sum_{n=1}^{N}\frac{\mu_0 I}{4\pi N}\frac{\sqrt{x^2+y^2}\bullet\cos(n\bullet\frac{2\pi}{N}) - R}{(z^2 + R^2 + x^2 + y^2 - 2R\sqrt{x^2+y^2}\bullet\cos(n\bullet\frac{2\pi}{N}))^{\frac{3}{2}}} \tag{8}$$

Using *matlab* to calculate the magnetic sensing intensity of the coil at each point in space, the magnetic field distribution of the circular coil at each point in space can be obtained by a bit of matrix operation in the space in which the entire coil is located. For observation, the $surf(x,y,B_h)$ function is used to obtain magnetic induction strength perpendicular to the Plane of the Z axis. Figure 2 is a magnetic induction intensity map of the plane where the coil is located using this method

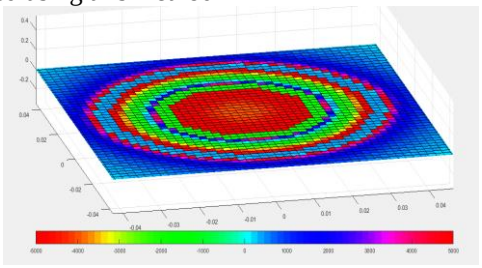

Figure 2. Magnetic induction intensity distribution of circular coils in X0Y-plane

As can be seen from the figure above, the magnetic induction strength of the circular coil is highly concentrated on the axis of the coil, and the high magnetic induction strength is also distributed in the area near the wire, and the magnetic induction strength is rapidly attenuated outside the circular coil.

III. MAGNETIC INDUCTION INTENSITY ANALYSIS OF DD COILS

A. *DD coil magnetic field distribution model*

DD-type coils can meet the current demand for high power, high charging spacing and anti-offset of charging coils, and DD coils combine the advantages of circular and flux coil designs to achieve the goal of increasing coupling efficiency by generating series flux located in the central area of the coil. The DD coil structure is based on the rectangular coil structure, so for the convenience of calculation, a model of a DD-type coil within the *xoy*-plane is established, as shown in Figure 3. Within the *xoy*-plane, the coordinates of the ends of the rectangular coil on the left side of the first side are: $A_{L1}(a,b)$, $B_{L1}(a,b')$, $C_{L1}(a',b)$, and $D_{L1}(a',b')$.

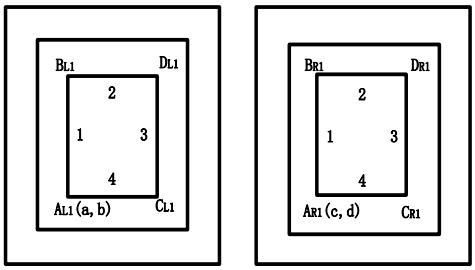

Figure 3. DD coil structure

According to the magnetic field distribution model of the DD coil, each wire in the DD coil is divided into N equivalents, and in solving, the magnetic field induction strength of each edge at each point in space is solved from the innermost point, and the magnetic field distribution of the entire DD coil is determined by the superposition principle. Magnetic induction strength B_{1L} on observation point $P(x,y,z)$ on the first side of the left rectangular coil is

$$\begin{cases} B_{P1}(x,y,z)=\sum_{n=1}^{N}\frac{\mu_0 I}{4\pi N}\cdot\frac{(b'-b)\cdot(x-a)}{\left((\text{x-a})^2+(\text{y-b-n}\cdot(\frac{b'-b}{N}))^2+z^2\right)^{\frac{3}{2}}} \\ B_{P2}(x,y,z)=\sum_{n=1}^{N}\frac{\mu_0 I}{4\pi N}\cdot\frac{(a'-a)\cdot(y-b')}{\left((\text{x-a-n}\cdot(\frac{a'-a}{N}))^2+(\text{y-b'})^2+z^2\right)^{\frac{3}{2}}} \\ B_{P3}(x,y,z)=\sum_{n=1}^{N}\frac{\mu_0 I}{4\pi N}\cdot\frac{(b'-b)\cdot(x-a')}{\left((\text{x-a'})^2+(\text{y-b-n}\cdot(\frac{b'-b}{N}))^2+z^2\right)^{\frac{3}{2}}} \\ B_{p4}(x,y,z)=\sum_{n=1}^{N}\frac{\mu_0 I}{4\pi N}\cdot\frac{(a'-a)\cdot(y-b)}{\left((\text{x-a-n}\cdot(\frac{a'-a}{N}))^2+(\text{y-b})^2+z^2\right)^{\frac{3}{2}}} \end{cases} \quad (9)$$

$$B_{1l}=B_{P1}(x,y,z)+B_{P2}(x,y,z)+B_{P3}(x,y,z)+B_{P4}(x,y,z) \quad (10)$$

Similarly, using the same solution, the magnetic induction intensity B_{1r} of the first coil in the right rectangular coil at the observation point P can be obtained, the magnetic induction intensity of each coil is solved according to the above method, and the magnetic induction intensity of the entire DD coil at the P point B can be obtained by using the superposition principle.

$$\begin{cases} B_1=B_{1l}+B_{1r} \\ B_2=B_{2l}+B_{2r} \\ B_3=B_{3l}+B_{3r} \end{cases} \quad (11)$$

$$B=B_1+B_2+B_3 \quad (12)$$

The magnetic field distribution of the DD coil at each point in the space is obtained by a bit of matrix operation in the space in which the entire coil is located. Figure 4 is a magnetic induction intensity map of the plane where the P-point is based, with the innermost length of the coil is 30mm, the width is 40mm, and the number of turns is 3, and the P-point to xoy plane is 50mm.

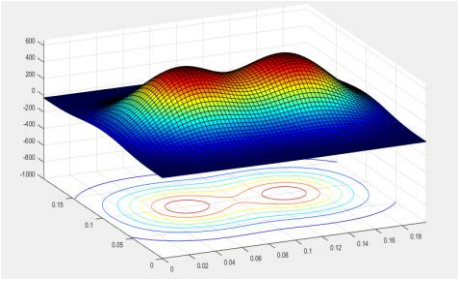

Figure 4. DD coil magnetic induction intensity map

According to the figure above, the DD coil has a larger magnetic field concentration area than the circular coil directly above the coil, which makes the receiving coil have a greater offset, which improves the reliability of the coil in practical applications, while ensuring the power transmit-ssion performance .

B. Analysis of magnetic field characteristics of DD coils

By comparison, several important design parameters in DD coil design are selected in this paper, and their influence on the transmission performance of coils is studied. The parameter distribution is shown in Figure 5

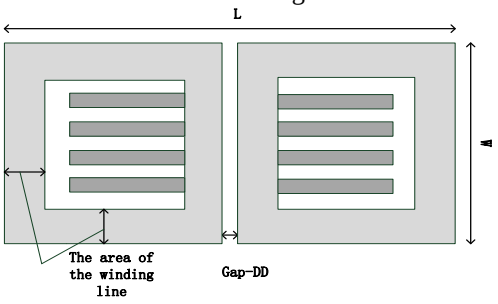

Figure 5. DD coil structure diagram

The area of the receiving coil is $S_s=L_s\cdot W_s$, L_s and W_s are the length and width of the receiving coil, and the transmit coil is $S_p=L_p\cdot W_p$. The overlay of the magnetic induction strength of all the grids in the face where S_s is located is B_{sum}, and the average value of the magnetic induction strength of all grids in the S_s face is B_E The effect son of the above parameters on B_{sum} and B_E is analyzed.

1) S : Area of DD coils

It can be seen by the superposition theorem that the number of turns is proportional to the magnetic induction strength in space, therefore, under the requirement of optimal transmission performance, the coil should be tightly

wound, and when wrapped, the area of the coil is mainly determined by the diameter, spacing and number of turns. When the emission coil size is $0.98m \times 0.54m$, and the wide Ws of the receiving coil is taken $0.45m$, $0.55m$, $0.65m$, respectively, the relationship between B_{sum} and B_E varies with L_s as shown in Figure 6

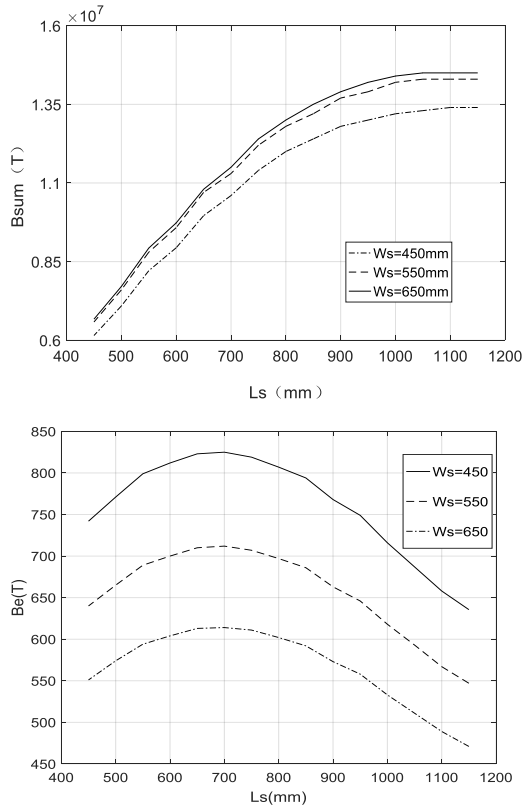

Figure 6. A-B diagram(With the emission coil size constant to A, the wide B of the receiving coil is taken C, D, E)

As can be seen from Figure 6, the emission coil size is certain, and as the receiving coil increases, B_{sum} will stabilize after increasing to a certain value. The average B_E of the magnetic induction strength in the receiving coil will gradually decay. B_{sum} and B_E reach the highest point when the coil parameters are optimal, which is the goal of optimizing the design

2) $\frac{L}{W}$ *:DD coil aspect ratio*

Because of the existence of the intermediate series flux path of the DD coil, the aspect ratio of the DD coil has a stronger and more complex effect on the spatial magnetic field strength distribution of the coil. At a certain size of the receiving coil, the area of the transmit coil is fixed, and the relationship between B_{sum} and B_E varies with the $\frac{L}{W}$ of the transmit coil as shown in Figure 7

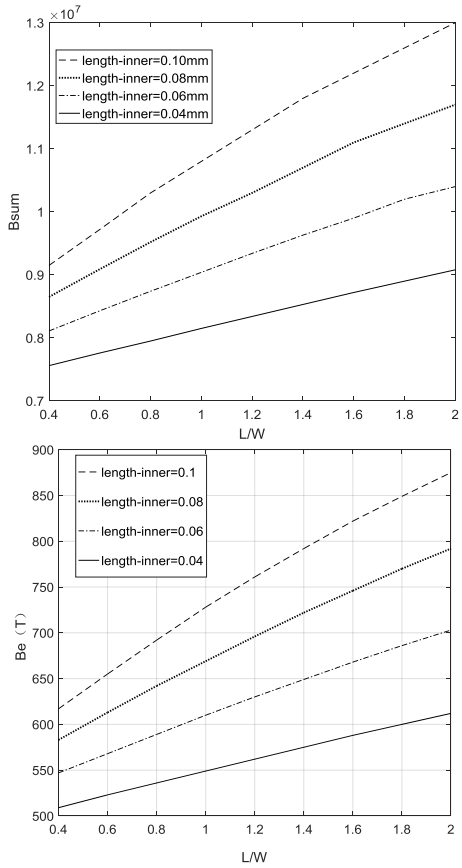

Figure 7. Relationship between $\frac{L}{W}$ and B_{sum}, B_E

As can be seen from Figure 7, the emission coil area is somewhat timed, and as $\frac{L}{W}$ increases, the coil becomes more and more "narrow", and both B_{sum} and B_E are gradually increasing. The enhanced effect of the series magnetic circuit in the middle of the DD coil on the magnetic field is described, but under the premise of considering the practicality of the coil, the charging coil "too narrow" will make the anti-offset characteristic of the charging coil worse and require more accurate position of the receiving coil. In the coil's magnetic induction strength improvement and to ensure its practicability, further parameter optimization is required to scientifically trade-off

3) Gap-*DD* *:Gap between two subcoils*

According to the flux management theory, the length of the flux tube that forms the series flux circuit is proportional to the height of the basic flux path, and when *G*ap-*DD* is too large, the magnetic induction strength of the magnetic field directly above the gap will decrease, and it is very likely that the coupling zero point will appear in the receiving coil. In the receiving coil size certain, the emission coil size is timely, B_{sum} and B_E with Gap-DD change relationship as shown in Figure 8

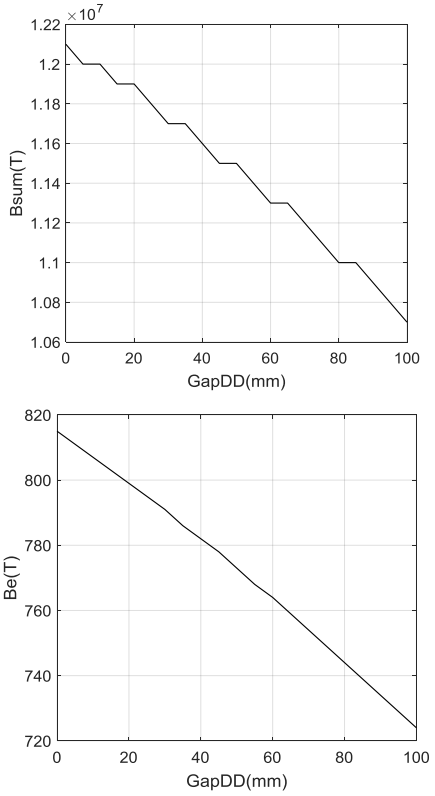

Figure 8. Relationship between *G*ap-*DD* and B_{sum}, B_E

As can be seen from Figure 8, B_{sum} and B_E show a decreasing trend as the *G*ap-*DD* of the launch coil increases. From the analysis, it can be seen that *G*ap-*DD* over the General Assembly weakens the magnetic induction strength above it, and even appears "coupling zero point", but based on flux management theory *G*ap-*DD* has an enhanced effect on the basic flux path height. In cases where the degree of influence of the two to the magnetic field cannot be quantified, other means need to be used to determine the parameters

In addition, in order to improve the efficiency of the transmission of electrical energy from the transmit coil, a high magnetic conductivity ferrite material can be added below the coil to produce a unipolar magnetic field, which increases the charging gap of the wireless charging system under the condition that the basic flux path height of the original coil is increased.

IV. SUMMARY AND OUTLOOK

In this paper, a magnetic field model of the coil is established for the circular and DD-type wireless charging coils, and the magnetic field distribution characteristics of the two coils are analyzed. The circular coil is simple in structure, the magnetic field is distributed in concentric circle in the horizontal plane, in the vertical direction, the magnetic field presents the axis high concentration trend, suitable for the scene of receiving coil is smaller than the transmit coil, the magnetic flux path of the DD coil is relatively high, can produce a larger effective coupling area with the receiving coil at the same height, and it is found through analysis that after the area of the receiving coil is larger than the transmit coil, the continued increase of the receiving coil area has little effect on transmission efficiency, increase the L/W of the transmit coil under the right position of the receiving coil, and can obtain a higher charging height under the same conditions, in addition, in order to avoid coupling zero points, the *G*ap-*DD* of the transmit coil should be as low as possible

Through the above results, the wireless charging coil design can provide a basic theoretical analysis method, the magnetic field distribution trend of the coil is pre-determined. But more precise design parameters, you need to quantify the impact of each parameter on coil performance, through the intelligent optimization algorithm to obtain.

ACKNOWLEDGMENT

This paper was supported by the Science and Technology Coordination Innovation Project Plan of Shannxi Province (No. 2015KTZDGY-02-01).

REFERENCES

[1] Zhao Zhengming, Liu Fang, Chen Kainan. A review of wireless charging technology for electric vehicles [J]. Transactions of China Electrotechnical Society, 2016, 31(20): 30-40.

[2] Mao Huan. Smart wireless charger design based on DSC [D]; Suzhou University, 2014.

[3] Zhu Chunbo, Jiang Jinhai, Song Kai, et al. Advances in the research on key technologies of dynamic wireless charging of electric vehicles [J]. Automation of Electric Power Systems, 2017, 41(02): 60-5+72.

[4] Wang Zhixuan, Wang Min, Gao Shixiang. Distribution and simulation of the strength value of space magnetic field near the electrified circular coil [J]. Computer Engineering and Design, 2007, 28(3): 706-9.

[5] Budhia M, Boys J T, Covic G A, et al. Development of a Single-Sided Flux Magnetic Coupler for Electric Vehicle IPT Charging Systems [J]. IEEE Transactions on Industrial Electronics, 2013, 60(1): 318-28.